ARTICLE

Homochiral D_4-symmetric metal–organic cages from stereogenic Ru(II) metalloligands for effective enantioseparation of atropisomeric molecules

Kai Wu[1,*], Kang Li[1,*], Ya-Jun Hou[1], Mei Pan[1], Lu-Yin Zhang[1], Ling Chen[1] & Cheng-Yong Su[1,2]

Absolute chiral environments are rare in regular polyhedral and prismatic architectures, but are achievable from self-assembly of metal–organic cages/containers (MOCs), which endow us with a promising ability to imitate natural organization systems to accomplish stereo-chemical recognition, catalysis and separation. Here we report a general assembly approach to homochiral MOCs with robust chemical viability suitable for various practical applications. A stepwise process for assembly of enantiopure $\Delta\Delta\Delta\Delta\Delta\Delta\Delta\Delta$- and $\Lambda\Lambda\Lambda\Lambda\Lambda\Lambda\Lambda\Lambda$-$Pd_6(RuL_3)_8$ MOCs is accomplished by pre-resolution of the Δ/Λ-Ru-metalloligand precursors. The obtained Pd–Ru bimetallic MOCs feature in large D_4-symmetric chiral space imposed by the predetermined Ru(II)-octahedral stereoconfigurations, which are substitutionally inert, stable, water-soluble and are capable of encapsulating a dozen guests per cage. Chiral resolution tests reveal diverse host–guest stereoselectivity towards different chiral molecules, which demonstrate enantioseparation ability for atropisomeric compounds with C_2 symmetry. NMR studies indicate a distinctive resolution process depending on guest exchange dynamics, which is differentiable between host–guest diastereomers.

The design and synthesis of discrete nanoscale metal–organic cages/containers (MOCs) with specific configurations and cavities applying directional bridging ligands and geometrically prefixed metals is emerging as an appealing topic in recent supramolecular coordination chemistry[1–3]. Among this, the controlled assembly of enantiopure chiral cages is of special importance because of their potential applications in stereoselective recognition, catalysis and enzyme mimics[4–11]. Since the chiral space in regular polyhedra only rarely presents in snub dodecahedron and snub cube (all other Platonic, Archimedean, prismatic and antiprismatic solids are achiral)[12,13], assembly of chiral polyhedral MOCs is usually achieved by introducing stereogenic centres into the faces, edges or vertices of a polyhedron to remove inversion and mirror symmetries. In this way, a number of homochiral MOCs of *T*-symmetry[14–19] have been constructed, whereas the chiral MOCs of *O*-symmetry or higher were proved to be more formidable because of more possible stereoisomers and the demand to transmit single chirality from more subcomponents[20,21]. In principle, the chirality of an MOC can be generated either by the organic stereocentres (such as chiral tetrahedral C*) or the metal stereogenic centres. The latter strategy provides a versatile platform for stereochemistry of MOCs because the plentiful metal coordination geometries can afford innumerable stereogenic metal centres for assembly of chiral structures even from achiral components in a supramolecular sense[22–24]. The overall MOC symmetry can be restricted or reduced by the stereochemical coupling between metal centres. For example, transfer of stereoconfiguration information between vertices of a tetrahedron enables absolute assembly[24] of homoconfigurational $\Delta\Delta\Delta\Delta$- or $\Lambda\Lambda\Lambda\Lambda$-cages based on the stereogenic tris-chelate metal centres[15–17]. However, the lability of metal–ligand exchange often causes enantiomerization between opposite enantiomers[25], and racemic mixture cannot be prevented during the assembly process. Resolution of the enantiopure product usually has to be accomplished with the aid of chiral auxiliaries to form diastereomers, and stabilization of the dynamic metal centre often needs synergistic effect[15–17].

An alternative way to construct stable and robust homochiral MOCs based on the stereogenic metal centres is to design a metalloligand[26] containing a stereoconfigurationally inert metal centre in lieu of the C* stereocentre in organic ligand. Formation of MOCs by virtue of various metalloligands has been achieved in many excellent lines of works[27–32], in which spontaneous resolution and geometric isomerism were observed[33–35], yet construction of enantiopure MOCs from predetermined chiral metalloligands remains unexplored. On the basis of the well-known stereochemistry of D_3-symmetric $[Ru(bpy)_3]^{2+}$- or $[Ru(phen)_3]^{2+}$-type compounds, which are widely explored in DNA interactions, asymmetric catalysis and supramolecular chiral assemblies[36–40], we initiated the design of $[Ru(phen)_3]^{2+}$-type metalloligand for homochiral MOC self-assembly[26]. Since the stereoconfiguration of such tri-chelate Ru-octahedral centres is substitutionally inert and stable in solution assembly and crystallization process, we expect that the predetermined chirality of the Ru metalloligands can direct the assembly of homochiral MOCs with sufficient stability in practical applications. Although stereoselective recognition and catalysis using chiral hosts has been well established[14–19,41,42], enantioseparation of racemic guest molecules by means of homochiral coordination cages remains a challenge. Only a few examples are known to achieve moderate to good diastereoselectivity[43–46], thus urging an extensive study to solve the common problems in this field; for example, (a) efficient resolution of enantiopure cages, (b) effective stabilization of cage stereochemistry and (c) high guest inclusion capacity (more than three guests per host). Herein we report a general approach to assemble homochiral MOCs without post resolution based on the pre-resolved stereogenic Ru-octahedral centres, offering huge cages capable of large amounts of guest encapsulation (>10 guests per host). Specifically, stereoselective separation of atropisomeric molecules rather than C*-based chiral compounds is achieved, and a dynamic resolution process based on differentiable guest exchange by formation of diastereomers is proposed.

Results

Assembly of enantiopure MOCs. We have previously assembled heteronuclear Δ/Λ-Pd$_6$(RuL$_3$)$_8$ MOCs racemate (hereafter assigned as **rac-Δ/Λ-MOCs-16**, Fig. 1) from the racemic RuL$_3$ metalloligands (**rac-Δ/Λ-3**), which show the shape of an octahedron (defined by Pd$_6$ centres) or a rhombic dodecahedron (defined by Pd$_6$Ru$_8$ centres)[26]. It was noted that the cage assembly proceeded in a homochiral manner, with each individual **MOC-16** integrating the same handed Δ- or Λ-**3** enantiomers to display either $\Delta\Delta\Delta\Delta\Delta\Delta\Delta\Delta$ or $\Lambda\Lambda\Lambda\Lambda\Lambda\Lambda\Lambda\Lambda$
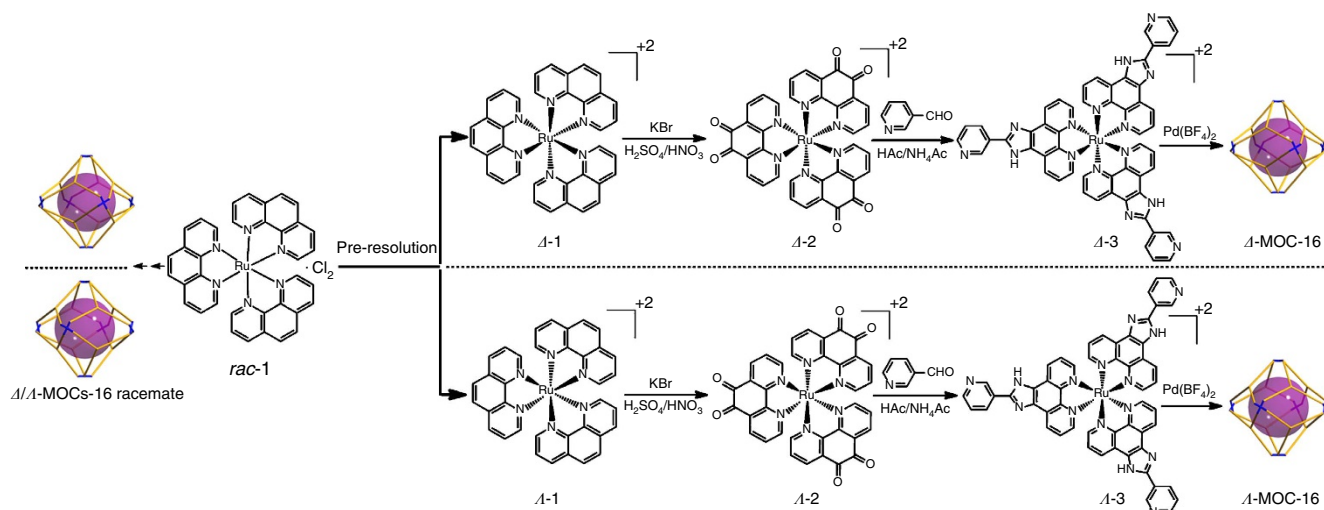
Figure 1 | Assembly procedures. Formation of racemic Δ/Λ-Pd$_6$(RuL$_3$)$_8$ cages (rac-Δ/Λ-MOCs-16) from mixed precursors, and stepwise syntheses of enantiopure Δ- and Λ-Pd$_6$(RuL$_3$)$_8$ cages (Δ-/Λ-MOCs-16) from pre-resolved Δ-3 and Λ-3 metalloligands.

homoconfigurations, indicative of strong cooperative stereo-chemical coupling between the metal centres[14–19,22–24] to direct the absolute self-organization[24] and exclusive formation of single homochiral Δ- or Λ-MOC-16. However, thus assembled chiral Δ- and Λ-MOCs co-crystallize simultaneously to give racemic products that are not ready for practical applications.

To make use of these homochiral cages, we started chiral resolution from well-established pre-resolution of Δ/Λ-[Ru(phen)$_3$]$^{2+}$ precursors and developed a pair of enantiomeric triangular metalloligands incorporating fixed chiral octahedral Ru(II) centres and pyridyl (Py) terminals ready for assembly of enantiopure Δ- and Λ-Pd$_6$(RuL$_3$)$_8$ MOCs separately. As shown in Fig. 1 and described in detail in Supplementary Figs 1–10, racemic Δ/Λ-[Ru(phen)$_3$]$^{2+}$ was first resolved into a pair of enantiomers (Δ- and Λ-1) in good yields using K$_2$[Sb$_2${(+)-tartrate}$_2$]·3H$_2$O as chiral induction agent, and then oxidized into Δ- and Λ-[Ru(Phendione)$_3$]$^{2+}$ (Δ- and Λ-2). With the aid of chiral shift reagent Eu((+)tfc)$_3$, the enantiopurity was tested to be 94.8% for Δ-1 and 95.3% for Λ-1 (ref. 47). The absolute configurations of the two pairs of Δ-/Λ-1 and Δ-/Λ-2 enantiomers have been well established by the single-crystal structural analyses (Supplementary Figs 1 and 2), which are in excellent agreement with the experimental resolution and syntheses. The phase purity of the bulk products of Δ-/Λ-1 and Δ-/Λ-2 enantiomers has also been verified using the powder X-ray diffraction measurements (Supplementary Figs 1 and 2). Further reaction of Δ- and Λ-2 with 3-pyridinecarboxaldehyde afforded a pair of stereogenic bulky Δ- and Λ-RuL$_3$ metalloligands (Δ- and Λ-3), and, finally, the coordination assembly of Δ- and Λ-3 enantiomers with Pd^{2+} ions unambiguously resulted in a pair of homochiral Δ- and Λ-Pd$_6$(RuL$_3$)$_8$ cages, namely Δ-MOC-16 and Λ-MOC-16, respectively. ^{1}H NMR spectra of two optically pure Δ-/Λ-MOCs-16 enantiomers give well-resolved proton patterns basically identical to previously reported racemic rac-Δ/Λ-MOCs-16 (Supplementary Fig. 8), showing distinguishable H resonance between the protons inside and outside cage (Supplementary Fig. 9). The ^{1}H-^{1}H-COSY and high-resolution mass spectrometry (HR-ESI-TOF-MS) have also been performed to verify formation of Pd$_6$(RuL$_3$)$_8$ cage structures (Supplementary Fig. 10).

The absolute configurational arrangement of the Δ- or Λ-3 metalloligands in Δ-MOC-16 or Λ-MOC-16, respectively, has been undoubtedly established by the single-crystal analyses (Supplementary Fig. 3). The single crystals of Δ-MOC-16 and Λ-MOC-16 were grown from their MeCN solutions in the presence of S-BINOL and R-BINOL, respectively, as absolute structural reference compounds for further authentication of the crystal chirality. Both Δ-MOC-16 and Λ-MOC-16 crystallize in the chiral space groups I422. In Δ-MOC-16, eight Δ-3 metalloligands are assembled by six square-coordinative Pd^{2+} ions to form Pd$_6$(RuL$_3$)$_8$ cage with the $\Delta\Delta\Delta\Delta\Delta\Delta\Delta\Delta$ homo-configurations (Fig. 2a). The crystal is packed by the identical Δ-MOC-16 cages in together with S-BINOL molecules, giving rise to enantiopure product with the absolute chirality exactly according to the chiral Δ-3 metalloligands and reference S-BINOL used in syntheses and crystal growth. In contrast, Λ-MOC-16 integrates eight Λ-3 metalloligands and six Pd^{2+} ions to form Pd$_6$(RuL$_3$)$_8$ cage with the $\Lambda\Lambda\Lambda\Lambda\Lambda\Lambda\Lambda\Lambda$ homoconfigurations (Fig. 2a), and co-crystallizes with R-BINOLs to result in enantiopure crystals. For both Δ-MOC-16 and Λ-MOC-16, the powder X-ray diffraction patterns of the bulk samples well match those of the single-crystal simulations, indicating satisfactory phase purity (Supplementary Fig. 3).

Careful examination of the crystal structures of Δ-/Λ-MOCs-16 enantiomers reveals that the cage molecule possesses crystal-lographically imposed D$_4$ symmetry (Fig. 2 and Supplementary Fig. 3). If regarding the cage as a pseudo-octahedron, the C$_4$ axis passes two vertices occupied by Pd1 ions, while two pairs of Pd2 ions are located on the C$_2$ axes. Therefore, the cage symmetry may be considered to degrade from chiral O-symmetry owing to disposition of the same handed Ru-stereocentres on eight faces of octahedron, or, on eight C$_3$ vertices of rhombic dodecahedron to impose $\Delta\Delta\Delta\Delta\Delta\Delta\Delta\Delta$ or $\Lambda\Lambda\Lambda\Lambda\Lambda\Lambda\Lambda\Lambda$ homoconfigurations in Δ-MOC-16 and Λ-MOC-16, respectively. In another word, the assembly of the homochiral Δ-/Λ-MOCs-16 enantiomers proceeds in a way of octahedral face-control or rhombic dodecahedral vertex-control, thus removing inversion i and mirror σ symmetries to turn an achiral O$_h$ group into a chiral D$_4$ group (Fig. 2c). Furthermore, the stereoconfigurations around six Pd^{2+} vertices are also induced by the fixed Ru-stereocentres. In Δ-MOC-16, six Pd-Py$_4$ subcomponents are all in Λ-configurations, with the four Py rings showing anticlock fan-like arrangement and vice versa in Λ-MOC-16. In contrast to other completely labile coordination cages[14–24], in the present cases, the stereoconfiguration around the Pd^{2+} corner is fixed by inserting Ru-stereocentres and cage integrity; therefore, enantiomerization through labile Pd-ligand exchange is inhibited for the whole cage. It is worth mentioning that eight S-BINOLs are captured by a Δ-MOC-16, or reversely, eight R-BINOLs by a Λ-MOC-16, on its window pockets but not completely into its cavity (Fig. 2b and Supplementary Figs 3a,b) probably because the crystallization takes place in the MeCN solution where hydrophobic effect is absent and the host–guest inclusion behaviour is different from that in aqueous medium discussed below (vide infra).

The circular dichroism (CD) spectra were also employed to monitor the whole synthetic and assembly processes to confirm that the absolute chirality of the starting Δ-/Λ-[Ru(phen)$_3$]$^{2+}$ pre-cursors were well preserved all the way down (Fig. 3 and Supplementary Fig. 11). In MeCN solution, Δ-/Λ-[Ru(phen)$_3$]$^{2+}$ mainly presents three absorption peaks at 225, 265 and 450 nm (Fig. 3a), with the first two corresponding to the n–$\pi^\star$ and π–$\pi^\star$ transitions of phen groups, while the last one originating from the metal-to-ligand charge transfer (MLCT) transition between Ru^{2+} and phen ligands. All three absorption bands are reflected in the corresponding CD spectra of the resolved Δ-1 and Λ-1 with the middle peak at 265 nm, giving the most prominent CD signal. Taking Δ-1 as an example, the same tendency of first negative and second positive Cotton effect from longer to shorter wavelength in the three CD bands is in accordance with the Δ-type octahedral chirality established for the Ru^{2+} coordination centre[48] and vice versa for the Λ-1 compound. For the rest three pairs of enantiomers, because of the cutoff effect of the solvents (dimethylsulphoxide (DMSO) or H$_2$O), the CD signals corresponding to the absorption at 225 nm were not fully presented; however, the other bands were clearly detected in the whole synthetic process, preserving the same chirality attributes for the same series of enantiomers (Δ-1, 2, 3, MOC-16 versus Λ-1, 2, 3, MOC-16, respectively). Furthermore, because of the accumulation effect (eightfold in Δ- or Λ-MOC-16 compared with Δ- or Λ-3) of multiple chiral Ru centres in one entity in the final enantiopure Δ-/Λ-MOCs-16, a remarkable increase in CD signal intensities was observed for Δ- or Λ-MOC-16 ($\Delta\varepsilon = \sim 720\,M^{-1}\,cm^{-1}$) in comparison with Δ- or Λ-3 ($\Delta\varepsilon = \sim 120\,M^{-1}\,cm^{-1}$). Optical rotation tests also manifested the absolute configurations in Δ- and Λ-MOCs-16 (Δ, $[\alpha]^{20}_D = -266°$; Λ, $[\alpha]^{20}_D = 272°$, $c = 0.5$, H$_2$O). From these CD studies we see that the stereochemistry of octahedral Ru centres is robust enough to survive all reaction conditions, exactly in agreement with the observations of chirality preservation in crystallographic study. The stereochemical stability of Δ- and Λ-MOCs-16 has also been testified against heating and longtime stay in solution (Fig. 3d), confirming that the absolute
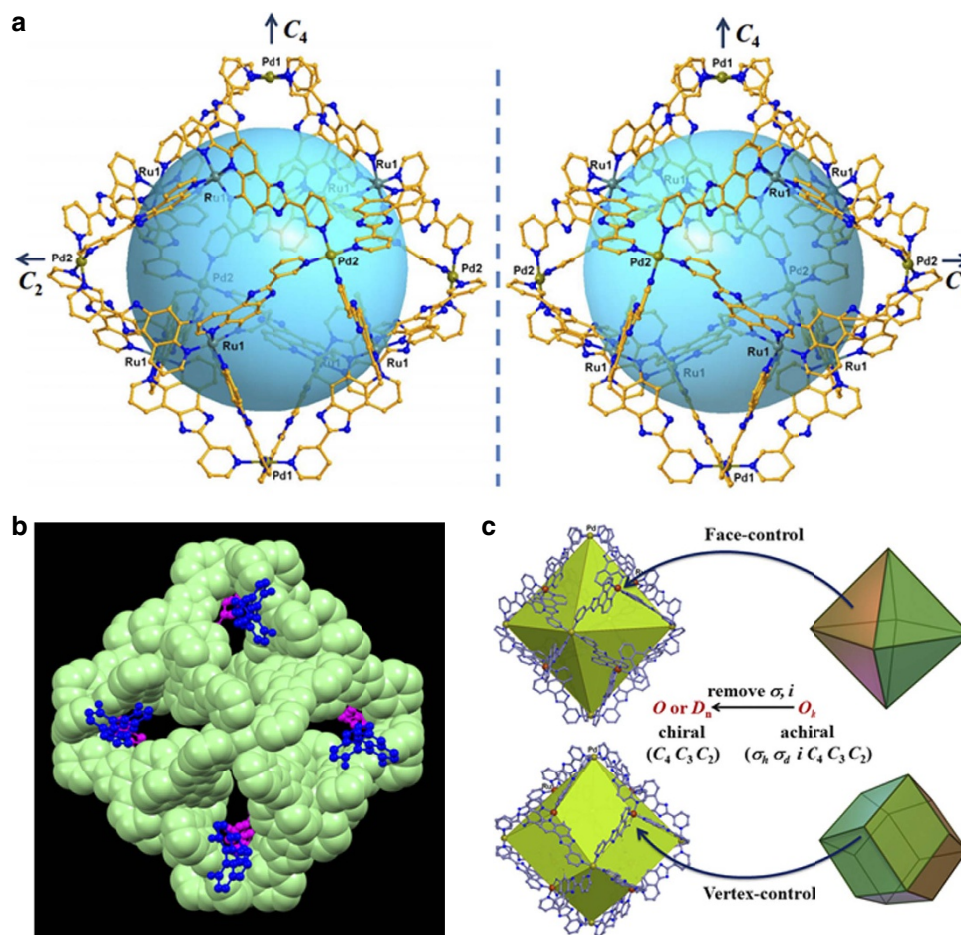
Figure 2 | Crystal structures. (**a**) A pair of D_4-symmetric homochiral Δ- and Λ-MOCs-16 showing $\Delta\Delta\Delta\Delta\Delta\Delta\Delta\Delta$ and $\Lambda\Lambda\Lambda\Lambda\Lambda\Lambda\Lambda\Lambda$ configurations of eight RuL$_3$ metalloligands whereas $\Lambda\Lambda\Lambda\Lambda\Lambda\Lambda$- and $\Delta\Delta\Delta\Delta\Delta\Delta$-configurations of six Pd-Py$_4$ subcomponents. (**b**) A Δ-MOC-16 cage (in space-filling mode) capturing eight S-BINOL guests (in ball-and-stick mode) on the windows pockets. (**c**) The demonstration how to form D_4 Λ-MOC-16 from O_h regular polyhedra by introducing eight Λ-3 metalloligands on the faces of an octahedron, or, on the C_3 vertices of a rhombic dodecahedron, to reduce molecular symmetry, and further direct Δ-arrangement of four pyridyl rings around six vertices of Pd centres.

chirality of each enantiomeric Δ- and Λ-MOC-16 is well retained on heating to 373 K and staying in solution for 50 days. Such a stable and substitutionally inert nature of stereogenic Ru centres plays a key role in fixing absolute chirality of Δ- and Λ-MOCs-16, despite intrinsic dynamics of Pd^{2+} centres subject to metal–ligand exchange, thereof paving the way for utilization of these enantiopure cages in, for example, stereoselective catalysis and separation.

Stereoselective separation of racemic guests. In an attempt to test enantioseparation ability of Δ-/Λ-MOC-16 cages, we selected two types of racemic organic molecules, one carrying a chiral C* centre and the other characteristic of C_2-symmetric chirality (Table 1). The host–guest inclusion examined by ^{1}H NMR in the D$_2$O system revealed that all chiral molecules can be well encapsulated by the **MOC-16** host owing to hydrophobic effect (Supplementary Figs 12–16), showing typical upfield shift of guest protons and further splitting of cage protons[26]. Moreover, the host–guest stereochemical relationship between enantiomeric Δ-/Λ-**MOCs-16** and R-/S-BINOLs has been examined using ^{1}H NMR enantiodifferentiation experiments, where two pairs of host–guest diastereomers, namely S-BINOL ⊂ Δ-**MOC-16**, R-BINOL ⊂ Δ-**MOC-16** and S-BINOL ⊂ Λ-**MOC-16**, R-BINOL ⊂ Λ-**MOC-16**, and two pairs of host–guest enantiomers, namely S-BINOL ⊂ Δ-**MOC-16**, R-BINOL ⊂ Λ-**MOC-16** and

R-BINOL ⊂ Δ-**MOC-16**, S-BINOL ⊂ Λ-**MOC-16**, are formed. As shown in Fig. 4, the solution dynamics is obviously distinguishable between the diastereomeric pairs, while that between the enantiomeric pairs is similar[41]. This means the homochiral Δ- and Λ-MOC-16 cages are able to recognize and differentiate R- and S-BINOL enantiomeric guests in solution because of their diastereomeric host–guest relationship. As a consequence, the chiral resolution of racemic molecules was carried out by Δ- and Λ-MOCs-16 separately in pure D$_2$O solution based on either a homogeneous or a heterogeneous method (see details in Methods or Supplementary Methods). The resolved guests were determined using high-performance liquid chromatography (HPLC) with enantiomeric excess (ee) averaged from three parallel experiments (Table 1 and Supplementary Figs 17–24).

The resolution results unveil that the homochiral Δ- or Λ-MOCs-16 have rather poor stereoselectivity towards chiral compounds containing C* stereocentres. As seen in Table 1, no obvious resolution effect can be detected for naproxen, 1-(1-naphthyl)ethanol and benzoin, despite ^{1}H NMR-proved inclusion of these guests by the host **MOC-16** (Supplementary Figs 14–16). However, through the same separation process, a pair of R-/S-BINOL atropisomers was successfully resolved, with the ee values reaching 34% or more by Δ-/Λ-**MOCs-16**. Relatively low enantioseparation results were obtained for R-/S-3-Br-BINOL
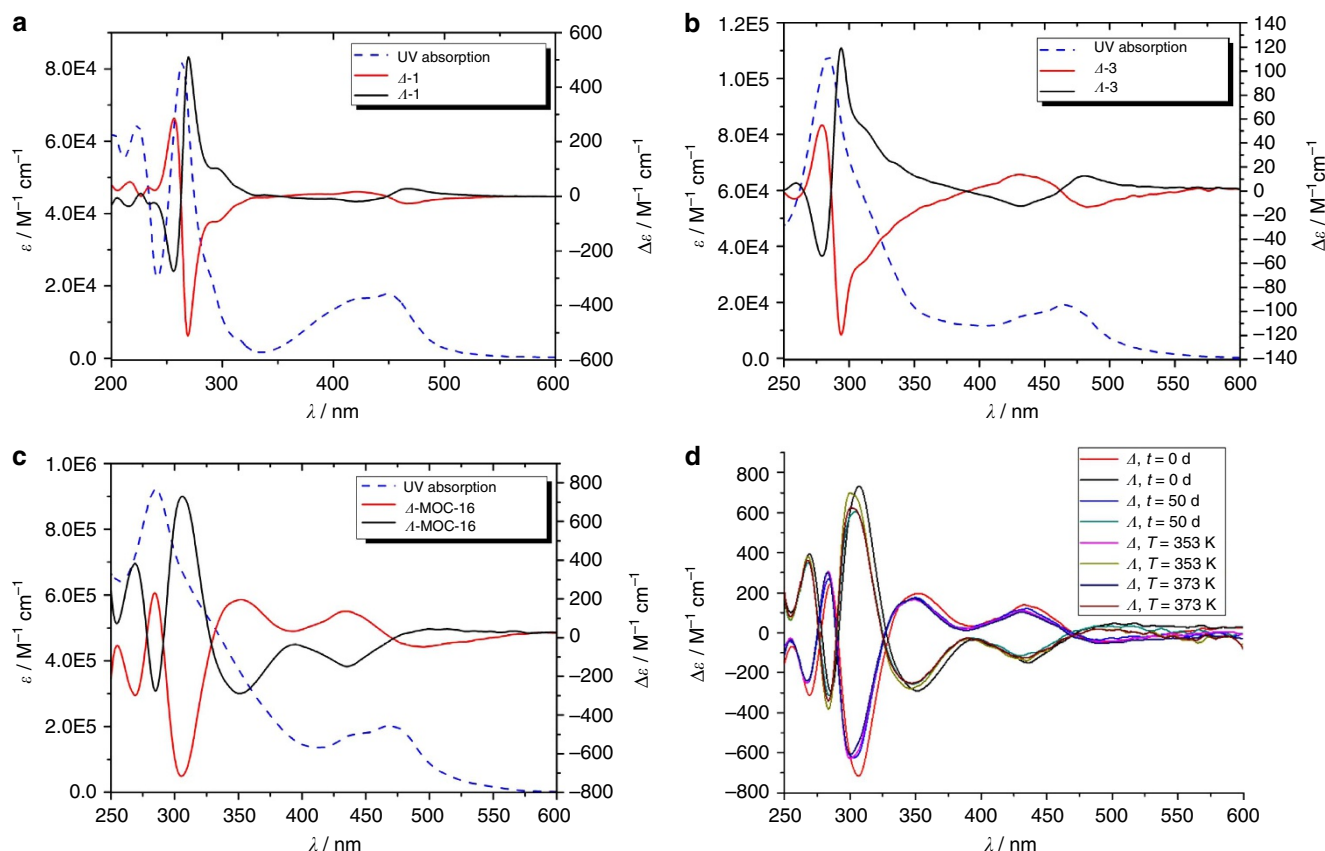
Figure 3 | CD and UV spectra. CD (solid lines) and ultraviolet (dotted lines). (**a**) Δ- and Λ-1 in MeCN, (**b**) Δ- and Λ-3 in DMSO, (**c**) Δ- and Λ-MOCs-16 in H$_2$O and (**d**) the stereochemical stability depending on time and temperature.

Table 1 | Enantioselective resolution of chiral organic molecules*.

Guests	Δ-MOC-16		Λ-MOC-16	
	R,S ratio	**ee (%)**	**R,S ratio**	**ee (%)**
BINOL	67:33	34	32:68	36
3-Br-BINOL	54:46	8	46:54	8
6-Br-BINOL	77:23	54	19:81	62
1,1'-spirobiindane-7,7'-diol	67:33	34	28:72	44
Naproxen	50:50	0	50:50	0
1-(1-Naphthyl)ethanol	51:50	1	50:50	0
Benzoin	50:50	0	50:50	0

ee, enantiomeric excess; MOC, metal–organic cage/container.
*The estimated uncertainty is about ± 2% as calculated for the averaged values from the results of three repeating resolution processes.

racemate; however, the resolution effect was greatly improved for the chiral discrimination of R-/S-6-Br-BINOL enantiomers. By applying Δ-**MOC-16**, the resolved product contains 77% of

R-isomer and 23% of S-isomer, giving an ee value of 54%. Surprisingly, an ee value up to 62% was obtained by Λ-**MOC-16** with the product dominant in S-isomer. Similar
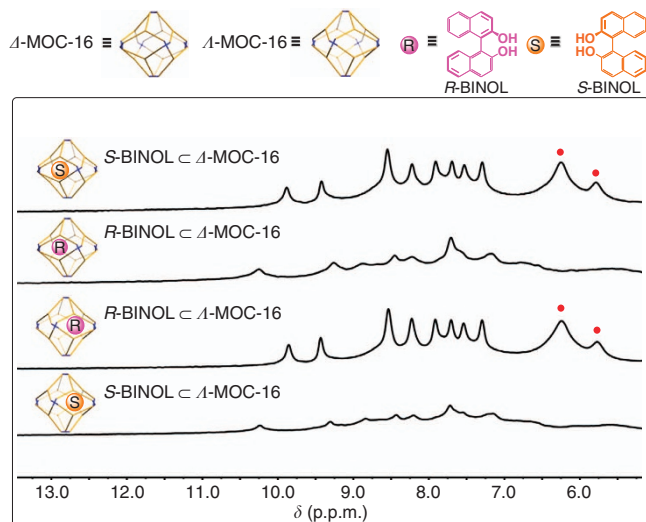
Figure 4 | ^{1}H NMR enantiodifferentiation experiments. Sequestration of enantiomeric R- or S-BINOL guests by homochiral $\varDelta$- or $\varLambda$-MOCs-16 (d_6-DMSO/D_2O = 1/5, 298 K). Red circles denote signals of encapsulated guests.

enantioseparation ability of $\varDelta$-/$\varLambda$-MOCs-16 was able to extend to another kind of atropisomeric compound R-/S-spirodiol, exhibiting the same host–guest stereoselectivity. The $\varDelta$-MOC-16 got 34% predominance of R-isomer, while a higher ee value of 44% was obtained for S-isomer by $\varLambda$-MOC-16. In general, $\varDelta$-MOC-16 shows a preferable stereoselectivity towards R-isomer, while $\varLambda$-MOC-16 prefers S-isomer for all chiral guests of C_2 symmetry. The higher-resolution effect from S-isomer $\subset \varLambda$-MOC-16 inclusion than from R-isomer $\subset \varDelta$-MOC-16 inclusion is unexpected, probably owing to the slight difference in optical attribute based on their optical rotation tests. To the best of our knowledge, such a preferable enantiorecognition of chiral guests with C_2 symmetry has not been observed before for cage compounds, and the enantioseparation ability of $\varDelta$-/$\varLambda$-MOCs-16 reaches high level within the known chiral organic and coordination cages[43–46,49]. In addition, the adequate solubility of MOCs-16 in water (2.6 g per 100 ml) makes it convenient to implement enantioseparation either in a homogeneous two-phase way (*Method I:* organic-water transfer as shown in Supplementary Fig. 25) or simply in a heterogeneous suspension way (*Method II:* solid-solution transfer as described in Methods). In comparison with the normally insoluble metal–organic frameworks for chiral separation, the water solubility of MOCs-16 offers advantages by using the hydrophobic effect to transfer water-insoluble organic guests into the aqueous phase, and the guest transformation between the organic-water phases is easy to accomplish. Extraction of the resolved chiral guests from the water phase of $\varDelta$-/$\varLambda$-MOCs-16 readily leads to recovery of the empty cages, which can be reused for the next runs of chiral resolution without a significant loss of the enantioseparation ability as tested by four cycles of R/S-6-Br-BINOL resolution with $\varDelta$-MOCs-16 (ee 51–57%, Supplementary Table 1). On the other hand, chiral resolution test of R/S-6-Br-BINOL racemate within $\varDelta$-MOC-16 and $\varLambda$-MOC-16 using 10 times the amount of host and guest indicates that the enantioselectivity is retained almost the same for the scaling up separation (ee 55 and 60%).

Resolution process study. To further understand the host–guest interactions for insight into the resolution mechanism, ^{1}H NMR titration was performed in an attempt to acquire association constants[42] for the pairs of host–guest diastereomers. However,

the experimental results obviously reveal intricate host–guest solution dynamics (Fig. 5 and Supplementary Figs 26–28). Since the MOC-16 cage has a huge molecular size (3.3 × 3.3 nm) and cavity (2895 Å^3 based on VOIDOO calculations) where a large amount of guests could be hosted (for example, 18 Phen guests per host)[26], the proton signals of both cage and guests are generally broadened and poorly resolved because of slow rotational diffusion and dynamics typical of large molecules, thereof preventing us from quantitative study with regard to thermodynamic or kinetic details by using the known methods for relatively simple host–guest systems (usually more than three guests per host)[50–53]. Nevertheless, it is evident that titration of enantiopure $\varLambda$-MOC-16 (or $\varDelta$-MOC-16) with R- and S-BINOL guests of C_2 symmetry undergoes remarkably different host–guest interaction processes, showing distinguishable guest inclusion behaviours for R- and S-BINOL atropisomers as demonstrated in Fig. 5a,b. This is in agreement with the observation from above-mentioned ^{1}H NMR enantiodifferentiation experiments because of the formation of a pair of host–guest diastereomers R-BINOL $\subset \varLambda$-MOC-16 and S-BINOL $\subset \varLambda$-MOC-16. In contrast, titration of $\varDelta$- and $\varLambda$-MOC-16 cages with the same C^*-chiral S-1-(1-naphthyl)ethanol guest, which should also give a pair of diastereomers S-1-(1-naphthyl)ethanol $\subset \varDelta$-MOC-16 and S-1-(1-naphthyl)ethanol $\subset \varLambda$-MOC-16, just results in rather similar ^{1}H NMR chemical shift patterns (Fig. 5d,e), indicating that the homochiral $\varLambda$-MOC-16 (or $\varDelta$-MOC-16) cage exhibits the same guest inclusion behaviours for R- and S-enantiomeric guests carrying C^* stereocentres.

As demonstrated in Fig. 5, stepwise inclusion of R-BINOLs by $\varLambda$-MOC-16 at 298 K causes inverse chemical shifts of cage protons, with those inside the cage moving upfield while those outside the cage moving downfield (Fig. 5a). The guest protons appear as severely broadened doublet and remain almost unmoved up to 12 guest inclusion. Addition of more than 12 equivalent R-BINOLs shows little influence on cage protons, but leads to downfield shift and further broadening of guest protons. These results suggest that at least 12 R-BINOLs are encapsulated inside the cage, and further guest uptake may speed up dynamic exchange. Inclusion of guests inside the cage is also supported with ^{1}H-^{1}H-COSY and NOESY measurements (Supplementary Fig. 26). For comparison, inclusion of S-BINOLs at 298 K does not lead to distinct bidirectional shifts of cage protons, while the resonance of guests is even broadened and becomes poorly visible together with the host protons on inclusion of more than 10 S-BINOLs (Fig. 5b). To observe guest signals more clearly, titration at a higher temperature 353 K was performed (Fig. 5c), which presents better resolved guest resonances but basically same overall chemical shift patterns as observed at 298. Therefore, similar host–guest interacting manners may be expected at these temperatures (*vide infra*). It is notable that the guest signals display a continuously downfield shift, characteristic of fast guest exchange. These NMR observations imply more dynamic host–guest interactions for S-BINOL $\subset \varLambda$-MOC-16 inclusion compared with R-BINOL $\subset \varLambda$-MOC-16 inclusion at the room temperature. Broadening of H resonance is indicative of slow and restricted molecular rotation and tumbling[54,55] as well as of a comparable guest exchange rate with the NMR timescale. For the S-BINOL $\subset \varLambda$-MOC-16 system, faster guest exchange dynamics may present, showing averaged influence on host protons either inside or outside. When the cage cavity is getting fulfilled (~ 12 guest per cage), the overall host–guest dynamics is slowed down to make NMR unable to discriminate resonating frequency. In contrast, guest exchange in the R-BINOL $\subset \varLambda$-MOC-16 system is slow enough at room temperature, thus showing distinguishable impact on host protons inside and outside. Such a guest dynamic difference between two host–guest diastereomers
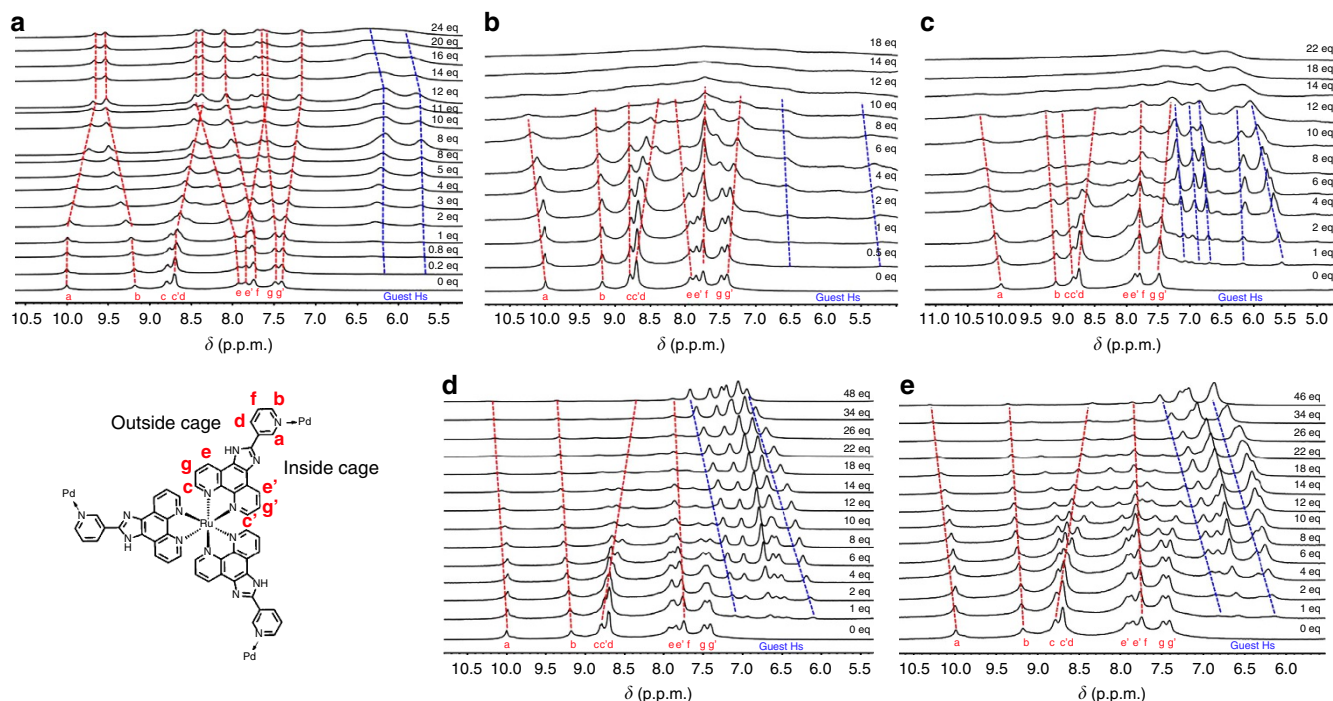
Figure 5 | ^{1}H NMR titration in DMSO-d_6/D$_2$O = 1/5. (**a**) R-BINOL $\subset$ Λ-MOC-16 at 298 K, (**b**) S-BINOL $\subset$ Λ-MOC-16 at 298 K, (**c**) S-BINOL $\subset$ Λ-MOC-16 at 353 K, (**d**) S-1-(1-naphthyl)ethanol $\subset$ Λ-MOC-16 at 298 K and (**e**) S-1-(1-naphthyl)ethanol $\subset$ Δ-MOC-16 at 298 K.

may account for the intrinsic factor that determines the enantioseparation ability of homochiral Δ- or Λ-MOCs-16 towards racemic R/S-BINOLs. On the contrary, titration of Δ- and Λ-MOCs-16 with S-1-(1-naphthyl)ethanol guests shows a similar guest exchange dynamics (Fig. 5d,e), where fast guest exchange is evident for both host–guest diastereomers. This may explain why the homochiral Δ-/Λ-MOCs-16s are unable to discriminate R/S-stereomers carrying opposite C* stereocentres. Although a confinement effect of a cage is usually expected to enhance the intrinsic chirality of the C* guests, discriminable stereoselectivity was not observed for the present C* molecules because of fast guest exchange.

Variable-temperature ^{1}H NMR study has been carried out to testify the above-proposed resolution process (Fig. 6 and Supplementary Fig. 29). It is clear that, for both R-BINOL $\subset$ Λ-MOC-16 and S-BINOL $\subset$ Λ-MOC-16 diastereomers, heating boosts guest dynamics and accelerates guest exchange, with two broadened signals getting better resolved and moving constantly downfield to approach free guests. This kind of host–guest solution dynamics might be comparable to the NMR-observable molecular dynamics[53–55]. However, the acceleration of the guest exchange dynamics from the sufficiently slow state to the fast state may not undergo a normal peak coalescence, but display a turning point where guest H resonances start to resolve apparently owing to NMR-observable freedom of guests from cage restriction. If taking the resonance frequency separation between two slowly restricted guest signals and the turning point of guest signal shifts for Eyring analysis, the guest exchange rates and energy barriers might be estimated at 1,021, 488 s^{-1} and 55.7, 60.5 kJ mol^{-1}, for S-BINOL $\subset$ Λ-MOC-16 and R-BINOL $\subset$ Λ-MOC-16 diastereomers, respectively. This means that Λ-MOC-16 can capture S-BINOL faster at lower energy cost than R-BINOL to accomplish a host–guest inclusion process.

Discussion

The host–guest dynamics and guest exchange mechanism have been vigorously explored for the insight of fundamental host–guest interactions and more complex encapsulation system design, in which both thermodynamics and kinetics play important roles in guest binding[50–55]. On the basis of above enantioseparation and NMR studies, we may speculate that the resolution process of homochiral Δ- or Λ-MOCs-16 towards chiral molecules of C_2 symmetry is mainly controlled by guest exchange dynamics, in comparison with the more popular thermodynamic resolution of racemic guests by chiral cages[43]. As demonstrated in Fig. 7, encapsulation of racemic R/S stereomers by, for example, Λ-MOC may proceed in a dynamic way depending on host–guest interactions and R/S-guest competition. If inclusion of S-stereomers is faster than R-stereomers via a lower guest exchange energy barrier, preferable resolution of S-stereomers over R-stereomers is achievable. It should be noted that such a dynamic resolution based on guest exchange dynamics might be comparable but inherently different from the well-known 'kinetic resolution' based on different reaction rates between a chiral catalyst and enantiomers[41,42,56]. Guest exchange and displacement process in a host–guest system is often sensitive to the synergistic effect from both thermodynamic and kinetic contributions[50–55]. Elongating resolution time may not influence ee results so much as by the catalytic kinetic resolution. We have tested the time-dependent chiral resolution of R/S-BINOL racemate by Λ-MOC-16. The results indicate an increase in the ee value within first 2 h, but remaining nearly unchanged afterwards (Supplementary Tables 2 and 3). We believe that the distinctive host–guest dynamics between R-BINOL $\subset$ Λ-MOC-16 and S-BINOL $\subset$ Λ-MOC-16 diastereomers should originate from the stereoconfigurations of the octahedral Ru centres. The twisted arrangement of three Phen motifs around Ru centres in helical sense may not be able to differentiate inclusion behaviour of configurationally free racemic guests carrying C* stereocentres, but significantly affect the interactions between Δ-/Λ-MOCs-16 and atropisomeric guests bearing C_2 symmetry owing to their intrinsic helical configurations. Formation of adaptive or mismatched host–guest diastereomers through dynamic guest exchange may be more
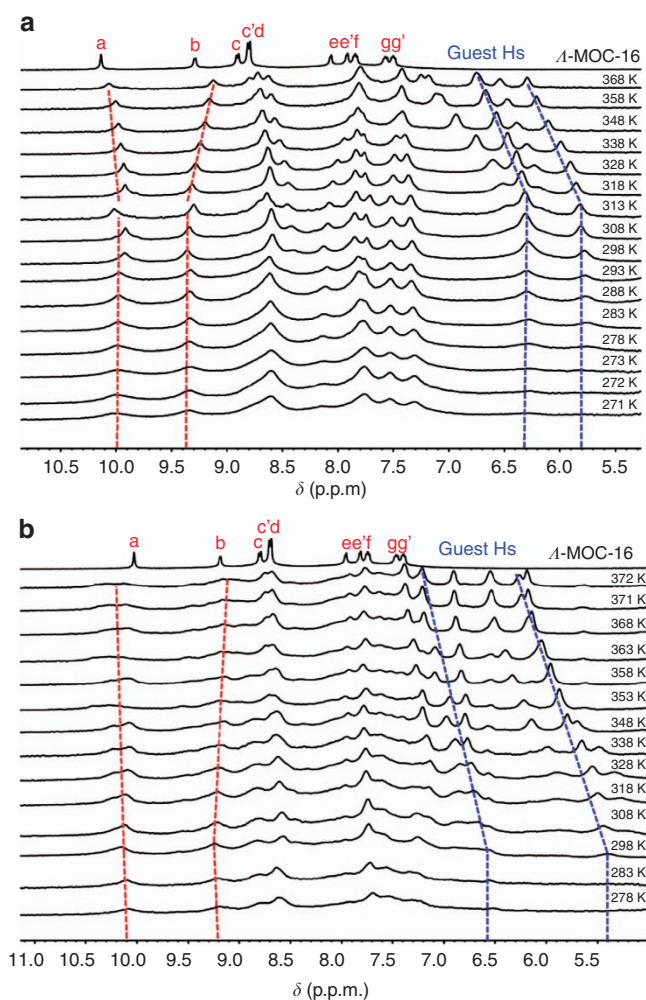
Figure 6 | VT ^1H NMR study of guest inclusion dynamics in solvent DMSO-d_6/D$_2$O = 1/5. (**a**) *R*-BINOL ⊂ *Λ*-MOC-16. (**b**) *S*-BINOL ⊂ *Λ*-MOC-16. Red lines show host protons, while blue lines show guest protons.

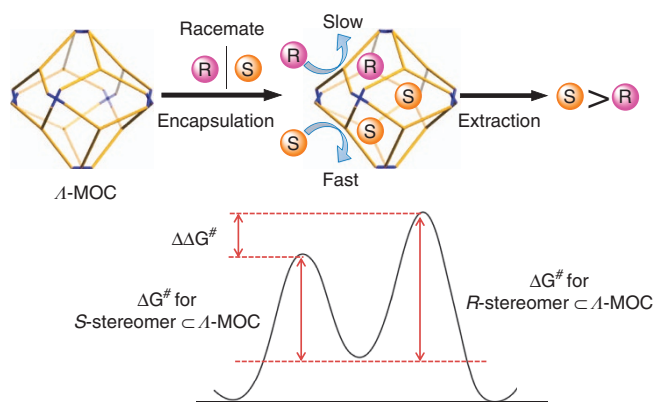**Figure 7 | Enantioseparation mechanism.** A possible resolution process relying on guest exchange dynamics of atropisomers with homochiral *Λ*-MOC-16. *Δ*G$^#$ represents guest exchange energy barrier.

dominated by stereochemical compatibility than by binding constant. Therefore, such stereoconfigurationally predetermined **MOCs** could afford better adaptive inclusion of one atropisomer over the opposite one, thus resulting in stereoselective separation.

In conclusion, pre-resolution of a pair of enantiomeric *Δ*-/*Λ*-Ru metalloligands has been successfully implemented based on the

stereogenic octahedral Ru centres in *Δ*-/*Λ*-[Ru(phen)$_3$]$^{2+}$ precursors, giving rise to the assembly of enantiopure D_4-symmetric *Δ*- and *Λ*-MOC-16 cages separately, which feature in high guest inclusion capacity and substantial stereochemical stability. The single-crystal diffraction analyses of the individual *Δ*- and *Λ*-MOC-16 cages verified the formation of absolute *ΔΔΔΔΔΔΔΔ*- and *ΛΛΛΛΛΛΛΛ* homoconfigurations, respectively, in corresponding Pd$_6$(RuL$_3$)$_8$ cages, and the crystallization of optically pure cage products. The stereoselective inclusion of chiral molecules has been tested for two kinds of organic racemates, that is, classic chiral compounds having C* centres and atropisomeric compounds characteristic of C_2 symmetry, with the phase transformation resolution processes. Successful enantioseparation of atropisomers has been accomplished by the use of these homochiral *Δ*- and *Λ*-MOCs-16, manifesting an unprecedented dynamic resolution process based on the kinetically driven guest exchange. The possible resolution mechanism has been investigated by the means of ^1H NMR titration, ^1H NMR enantiodifferentiation experiments as well as variable-temperature ^1H NMR study. In general, this kind of assembly process may provide a new platform to study the stereochemical transmission of optically stable metal centres to versatile homochiral entities in coordination chemistry, and the dynamic resolution behaviour imposed by stereoconfiguration of metal centres might be useful in various chiral resolution of synthetic and industrial significance.

Methods

Materials and measurements. Unless otherwise stated, all commercial reagents and solvents were used as commercially purchased without additional purification. The NMR spectra were recorded on Bruker AVANCE III 400 (400 MHz). Circular dichroism spectra and ultraviolet–visible absorption spectra were measured with a JASCO J-810 spectropolarimeter. Specific rotations were recorded on ADP440 + B + S. HR-ESI-TOF mass spectra were tested on Bruker Maxis 4G, and data analyses were processed with the Bruker Data Analysis software. HPLC spectra were measured on Agilent-2000. Diffraction data for the single crystals were collected on an Agilent SuperNova X-ray diffractometer using micro-focus dual X-ray sources (Supplementary Data 1). Syntheses and characterization details for all compounds are given in Supplementary Methods. Selected bond lengths (Å) and bond angles (°) are listed in Supplementary Tables 4–9.

Crystal data for {*Λ*-[Pd$_6$(RuL$_3$)$_8$](*S*-BINOL)$_4$}·anion·solvent (*Λ*-MOC-16).
$I422$ space group, $a = 32.2284(4)$ Å, $c = 38.2801(7)$ Å, $V = 39,760.5(13)$ Å^3, $Mr = 9,727.82$, $Dx = 0.813$ g cm^{-3}, $Z = 2$, $\mu = 2.599$ mm^{-1}, 16,396 independent reflections, of which 9,021 observed ($I > 2\sigma(I)$), $R_1 = 0.0711$, $wR_2 = 0.2375$, $S = 1.008$, Flack parameter = 0.131(13).

Crystal data for {*Λ*-[Pd$_6$(RuL$_3$)$_8$](*R*-BINOL)$_4$}·anion·solvent (*Λ*-MOC-16).
$I422$ space group, $a = 32.5722(6)$ Å, $c = 38.7258(9)$ Å, $V = 41,086.1(19)$ Å^3, $Mr = 9,727.82$, $Dx = 0.786$ g cm^{-3}, $Z = 2$, $\mu = 2.515$ mm^{-1}, 17,111 independent reflections, of which 7,718 observed ($I > 2\sigma(I)$), $R_1 = 0.0913$, $wR_2 = 0.2680$, $S = 1.038$, Flack parameter = 0.139(16).

Crystal data for {*Δ*-[Ru(Phen)$_3$](PF$_6$)$_2$}$_2$·(C$_6$H$_5$CH$_3$)·(CH$_3$CN)$_2$ (*Δ*-1).
$P4_1$ space group, $a = 25.5619(2)$ Å, $c = 12.5769(2)$ Å, $V = 8,217.88(18)$ Å^3, $Mr = 2,037.48$, $Dx = 1.647$ g cm^{-3}, $Z = 4$, $\mu = 0.556$ mm^{-1}, 19,736 independent reflections, of which 17,221 observed ($I > 2\sigma(I)$), $R_1 = 0.0678$, $wR_2 = 0.1759$, $S = 1.050$, Flack parameter = 0.00(4).

Crystal data for {*Λ*-[Ru(Phen)$_3$](PF$_6$)$_2$}$_2$·(C$_6$H$_5$CH$_3$)·(CH$_3$CN)$_2$ (*Λ*-1).
$P4_3$ space group, $a = 25.5802(1)$ Å, $c = 12.5709(1)$ Å, $V = 8,225.73(9)$ Å^3, $Mr = 2,037.48$, $Dx = 1.645$ g cm^{-3}, $Z = 4$, $\mu = 0.556$ mm^{-1}, 20,142 independent reflections, of which 17,755 observed ($I > 2\sigma(I)$), $R_1 = 0.0408$, $wR_2 = 0.1071$, $S = 1.025$, Flack parameter = $-0.033(8)$.

Crystal data for *Δ*-[Ru(Phendione)$_3$](ClO$_4$)$_2$·(H$_2$O)·(CH$_3$CN)$_2$ (*Δ*-2).
$P2_12_12_1$ space group, $a = 13.8114(2)$ Å, $b = 14.0525(2)$ Å, $c = 20.7957(3)$ Å, $V = 4,036.13(10)$ Å^3, $Mr = 1,028.64$, $Dx = 1.693$ g cm^{-3}, $Z = 4$, $\mu = 5.107$ mm^{-1}, 7,890 independent reflections, of which 7,536 observed ($I > 2\sigma(I)$), $R_1 = 0.0438$, $wR_2 = 0.1195$, $S = 1.025$, Flack parameter = $-0.015(4)$.

Crystal data for Λ-[Ru(Phendione)$_3$](ClO$_4$)$_2 \cdot$(H$_2$O)$\cdot$(CH$_3$CN)$_2$ (Λ-2).

$P2_12_12_1$ space group, $a = 13.7734(2)$ Å, $b = 14.0148(2)$ Å, $c = 20.7100(3)$ Å, $V = 3,997.68(10)$ Å^3, $Mr = 1,022.59$, $Dx = 1.699$ g cm^{-3}, $Z = 4$, $\mu = 5.156$ mm^{-1}, 7,980 independent reflections, of which 7,737 observed ($I > 2\sigma(I)$), $R_1 = 0.0409$, $wR_2 = 0.1084$, $S = 1.032$, Flack parameter $= -0.011(3)$.

General chiral resolution of racemic guests by enantiopure Δ/Λ-MOCs-16.
Two kinds of methods were used to resolve racemic guests depending on whether the guest inclusion leads to precipitation. For racemic R/S-BINOL, R/S-3-Br-BINOL, R/S-6-Br-BINOL and R/S-naproxen molecules, *Method I* based on a solution–solution transfer was applied to avoid host–guest precipitation (Supplementary Fig. 25). An aqueous solution of Δ- or Λ-MOC-16 and an ethereal solution of racemic guest were mixed and stirred vigorously at room temperature, and then the bottom layer was taken out and extracted with CHCl$_3$. The extractants were combined and the solvent was removed using rotary evaporator to afford white solid as resolved guests by the homochiral MOC host. The solid was redissolved in isopropanol and the ee of guest molecules was determined using HPLC. For racemic R/S-spirodiol, R/S-1-(naphthyl)ethanol and R/S-benzoin molecules, Method II based on a solid-solution transfer was applied directly. The powder of guest racemate was suspended in the aqueous solution of Δ-or Λ-MOC-16. The mixture was stirred vigorously at room temperature. After centrifugation, the filtrate was collected and extracted with CHCl$_3$. The extractants were combined and the solvent was removed by rotary evaporator to afford white solid as resolved guest. The ee analysis is the same as in Method I.

References

1. Amouri, H., Desmarets, C. & Moussa, J. Confined nanospaces in metallocages: guest molecules, weakly encapsulated anions, and catalyst sequestration. *Chem. Rev.* **112**, 2015–2041 (2012).
2. Cook, T. R., Zheng, Y.-R. & Stang, P. J. Metal–organic frameworks and self-assembled supramolecular coordination complexes: comparing and contrasting the design, synthesis, and functionality of metal–organic materials. *Chem. Rev.* **113**, 734–777 (2013).
3. Meng, W. et al. A self-assembled M$_8$L$_6$ cubic cage that selectively encapsulates large aromatic guests. *Angew. Chem. Int. Ed.* **50**, 3479–3483 (2011).
4. Smulders, M. M. J., Riddell, I. A., Browne, C. & Nitschke, J. R. Building on architectural principles for three-dimensional metallosupramolecular construction. *Chem. Soc. Rev.* **42**, 1728–1754 (2013).
5. Pluth, M. D., Bergman, R. G. & Raymond, K. N. Proton-mediated chemistry and catalysis in a self-assembled supramolecular host. *Acc. Chem. Res.* **42**, 1650–1659 (2009).
6. Nishioka, Y., Yamaguchi, T., Kawano, M. & Fujita, M. Asymmetric [2 + 2] olefin cross photoaddition in a self-assembled host with remote chiral auxiliaries. *J. Am. Chem. Soc.* **130**, 8160–8161 (2008).
7. Argent, S. P., Riis-Johannessen, T., Jeffery, J. C., Harding, L. P. & Ward, M. Diastereoselective formation and optical activity of an M$_4$L$_6$ cage complex. *Chem. Commun.* 4647–4649 (2005).
8. Ousaka, N. et al. Efficient long-range stereochemical communication and cooperative effects in self-assembled Fe$_4$L$_6$ cages. *J. Am. Chem. Soc.* **134**, 15528–15537 (2012).
9. Dong, J., Zhou, Y., Zhang, F. & Cui, Y. A highly fluorescent metallosalalen-based chiral cage for enantioselective recognition and sensing. *Chem. Eur. J.* **20**, 6455–6461 (2014).
10. Wang, J., He, C., Wu, P. Y., Wang, J. & Duan, C. Y. An amide-containing metal–organic tetrahedron responding to a spin-trapping reaction in a fluorescent enhancement manner for biological imaging of NO in living cells. *J. Am. Chem. Soc.* **133**, 12402–12405 (2011).
11. Samanta, D. & Mukherjee, S. P. Component selection in the self-assembly of palladium(II) nanocages and cage-to-cage transformations. *Chem. Eur. J.* **20**, 12483–12492 (2014).
12. MacGillivray, L. R. & Atwood, J. L. Structural classification and general principles for the design of spherical molecular hosts. *Angew. Chem. Int. Ed.* **38**, 1018–1033 (1999).
13. Hamilton, T. D. & MacGillivray, L. R. Enclosed chiral environments from self-assembled metal-organic polyhedral. *Cryst. Growth Des.* **4**, 419–430 (2004).
14. Stang, P. J. & Olenyuk, B. Transition-metal-mediated rational design and self-assembly of chiral, nanoscale supramolecular polyhedra with unique T symmetry. *Organometallics* **16**, 3094–3096 (1997).
15. Ousaka, N., Clegg, J. K. & Nitschke, J. R. Nonlinear enhancement of chiroptical response through subcomponent substitution in M$_4$L$_6$ cages. *Angew. Chem. Int. Ed.* **51**, 1464–1468 (2012).
16. Davis, A. V., Fiedler, D., Ziegler, M., Terpin, A. & Raymond, K. N. Resolution of chiral, tetrahedral M$_4$L$_6$ metal-ligand hosts. *J. Am. Chem. Soc.* **129**, 15354–15363 (2007).
17. Terpin, A. J., Ziegler, M., Johnson, D. W. & Raymond, K. N. Resolution and kinetic stability of a chiral supramolecular assembly made of labile components. *Angew. Chem. Int. Ed.* **40**, 157–160 (2001).
18. Meng, W., Clegg, J. K., Thoburn, J. D. & Nitschke, J. R. Controlling the transmission of stereochemical information through space in terphenyl-edged Fe$_4$L$_6$ cages. *J. Am. Chem. Soc.* **133**, 13652–13660 (2011).
19. Schweiger, M., Seidel, S. R., Schmitz, M. & Stang, P. J. Rational design of chiral nanoscale adamantanoids. *Org. Lett.* **2**, 1255–1257 (2000).
20. Gütz, C. et al. Enantiomerically pure [M$_6$L$_{12}$] or [M$_{12}$L$_{24}$] polyhedra from flexible bis(pyridine) ligands. *Angew. Chem. Int. Ed.* **53**, 1693–1698 (2014).
21. Yang, Y. et al. Diastereoselective synthesis of O symmetric heterometallic cubic cages. *Chem. Commun.* **51**, 3804–3807 (2015).
22. Knof, U. & von Zelewsky, A. Predetermined chirality at metal centers. *Angew. Chem. Int. Ed.* **38**, 302–322 (1999).
23. Castilla, A. M., Ramsay, W. J. & Nitschke, J. R. Stereochemistry in subcomponent self-assembly. *Acc. Chem. Res.* **47**, 2063–2073 (2014).
24. Northrop, B. H., Zheng, Y.-R., Chi, K.-W. & Stang, P. J. Self-organization in coordination-driven self-assembly. *Acc. Chem. Res.* **42**, 1554–1563 (2009).
25. Saalfrank, R. W. et al. Enantiomerisation of tetrahedral homochiral [M$_4$L$_6$] clusters: synchronised four bailar twists and six atropenantiomerisation processes monitored by temperature-dependent dynamic ^{1}H NMR spectroscopy. *Chem. Eur. J.* **8**, 2679–2683 (2002).
26. Li, K. et al. Stepwise assembly of Pd$_6$(RuL$_3$)$_8$ nanoscale rhombododecahedral metal–organic cages via metalloligand strategy for guest trapping and protection. *J. Am. Chem. Soc.* **136**, 4456–4459 (2014).
27. Garrison, J. C. et al. Synthesis and characterization of a trigonal bipyramidal supramolecular cage based upon rhodium and platinum metal centers. *Chem. Commun.* 4644–4646 (2006).
28. Smulders, M. M. J., Jiménez, A. & Nitschke, J. R. Integrative self-sorting synthesis of a Fe$_8$Pt$_6$L$_{24}$ cubic cage. *Angew. Chem. Int. Ed.* **51**, 6681–6685 (2012).
29. Hiraoka, S., Sakata, Y. & Shionoya, M. Ti(IV)-centered dynamic interconversion between Pd(II), Ti(IV)-containing ring and cage molecules. *J. Am. Chem. Soc.* **130**, 10058–10059 (2008).
30. Sakata, Y., Hiraoka, S. & Shionoya, M. Site-selective ligand exchange on a heteroleptic Ti^{IV} complex towards stepwise multicomponent self-assembly. *Chem. Eur. J.* **16**, 3318–3325 (2010).
31. Kryschenko, Y. K., Seidel, S. R., Arif, A. M. & Stang, P. J. Coordination-driven self-assembly of predesigned supramolecular triangles. *J. Am. Chem. Soc.* **125**, 5193–5198 (2003).
32. Li, H., Yao, Z.-J., Liu, D. & Jin, G.-X. Multi-component coordination-driven self-assembly toward heterometallic macrocycles and cages. *Coord. Chem. Rev.* **293**, 139–157 (2015).
33. Wu, H.-B. & Wang, Q.-M. Construction of heterometallic cages with tripodal metalloligands. *Angew. Chem. Int. Ed.* **48**, 7343–7345 (2009).
34. Metherell, A. J. & Ward, M. D. Stepwise assembly of an adamantoid Ru$_4$Ag$_6$ cage by control of metal coordination geometry at specific sites. *Chem. Commun.* **50**, 10979–10982 (2014).
35. Zhou, X.-P. et al. A high-symmetry coordination cage from 38- or 62-component self-assembly. *J. Am. Chem. Soc.* **134**, 8042–8045 (2012).
36. Carlucci, L., Ciani, G., Maggini, S., Proserpio, D. M. & Visconti, M. Heterometallic modular metal-organic 3D frameworks assembled via new tris-beta-diketonate metalloligands: nanoporous materials for anion exchange and scaffolding of selected anionic guests. *Chem. Eur. J.* **16**, 12328–12341 (2010).
37. Hamelin, O., Rimboud, M., Pecaut, J. & Fontecave, M. Chiral-at-metal ruthenium complex as a metalloligand for asymmetric catalysis. *Inorg. Chem.* **46**, 5354–5360 (2007).
38. Hiort, C., Lincoln, P. & Norden, B. DNA binding of Δ- and Λ-[Ru(phen)$_2$DPPZ]$^{2+}$. *J. Am. Chem. Soc.* **115**, 3448–3454 (1993).
39. Smith, J. A., Collins, J. G., Patterson, B. T. & Keene, F. R. Total enantioselectivity in the DNA binding of the dinuclear ruthenium (II) complex [{Ru(Me$_2$bpy)$_2$}$_2$(μ-bpm)]$^{4+}$ {bpm = 2,2′-bipyrimidine. Me$_2$bpy = 4,4′-dimethyl-2,2′-bipyridine}. *Dalton Trans.* **9**, 1277–1283 (2004).
40. MacDonnell, F. M., Kim, M. J. & Bodige, S. Substitutionally inert complexes as chiral synthons for stereospecific supramolecular syntheses. *Coord. Chem. Rev.* **185**, 535–549 (1999).
41. Zhao, C. et al. Chiral amide directed assembly of a diastereo- and enantiopure supramolecular host and its application to enantioselective catalysis of neutral substrates. *J. Am. Chem. Soc.* **135**, 18802–18805 (2013).
42. Kida, T., Iwamoto, T., Asahara, H., Hinoue, T. & Akashi, M. Chiral recognition and kinetic resolution of aromatic amines via supramolecular chiral nanocapsules in nonpolar solvent. *J. Am. Chem. Soc.* **135**, 3371–3374 (2013).
43. Fiedler, D., Leung, D. H., Bergman, R. G. & Raymond, K. N. Enantioselective guest binding and dynamic resolution of cationic ruthenium complexes by a chiral metal-ligand assembly. *J. Am. Chem. Soc.* **126**, 3674–3675 (2004).
44. Hastings, C. J., Pluth, M. D., Biros, S. M., Bergman, R. G. & Raymond, K. N. Simultaneously bound guests and chiral recognition: a chiral self-assembled supramolecular host encapsulates hydrophobic guests. *Tetrahedron* **64**, 8362–8367 (2008).

45. Sawada, T., Matsumoto, A. & Fujita, M. Coordination-driven folding and assembly of a short peptide into a protein-like two-nanometer-sized channel. *Angew. Chem. Int. Ed.* **53,** 7228–7232 (2014).

46. Liu, T. F., Liu, Y., Xuan, W. M. & Cui, Y. Chiral nanoscale metal–organic tetrahedral cages: diastereoselective self-assembly and enantioselective separation. *Angew. Chem. Int. Ed.* **49,** 4121–4124 (2010).

47. Torres, A. S., Maloney, D. J., Tate, D., Saad, Y. & MacDonnell, F. M. Retention of optical activity during conversion of Λ-[Ru(1,10-phenanthroline)$_3$]$^{2+}$ to Λ-[Ru(1,10-phenanthroline-5,6-dione)$_3$]$^{2+}$ and Λ-[Ru(dipyrido[a:3,2-h:2',3'-c-]-phenazine)$_3$]$^{2+}$. *Inorg. Chim. Acta* **293,** 37–43 (1999).

48. McGee, K. A. & Mann, K. R. Inefficient crystal packing in chiral [Ru(phen)$_3$](PF$_6$)$_2$ enables oxygen molecule quenching of the solid-state MLCT emission. *J. Am. Chem. Soc.* **131,** 1896–1902 (2009).

49. Chen, L. *et al.* Separation of rare gases and chiral molecules by selective binding in porous organic cages. *Nat. Mater.* **13,** 954–960 (2014).

50. Smulders, M. M. J., Zarra, S. & Nitschke, J. R. Quantitative understanding of guest binding enables the design of complex host-guest behavior. *J. Am. Chem. Soc.* **135,** 7039–7046 (2013).

51. Zarra, S., Smulders, M. M. J., Lefebvre, Q., Clegg, J. K. & Nitschke, J. R. Guanidinium binding modulates guest exchange within an [M$_4$L$_6$] capsule. *Angew. Chem. Int. Ed.* **51,** 6882–6885 (2012).

52. Jiang, W., Ajami, D. & Rebek, Jr J. Alkane lengths determine encapsulation rates and equilibria. *J. Am. Chem. Soc.* **134,** 8070–8073 (2012).

53. Davis, A. V. *et al.* Guest exchange dynamics in an M$_4$L$_6$ tetrahedral host. *J. Am. Chem. Soc.* **128,** 1324–1333 (2006).

54. Mugridge, J. S., Szigethy, G., Bergman, R. G. & Raymond, K. N. Encapsulated guest-host dynamics: guest rotational barriers and tumbling as a probe of host interior cavity space. *J. Am. Chem. Soc.* **132,** 16256–16264 (2010).

55. Wang, B.-Y. *et al.* The entrapment of chiral guests with gated baskets: can a kinetic discrimination of enantiomers be governed through gating? *Chem. Eur. J.* **19,** 4767–4775 (2013).

56. Ma, G., Deng, J. & Sibi, M. P. Fluxionally chiral DMAP catalysts: kinetic resolution of axially chiral biaryl compounds. *Angew. Chem. Int. Ed.* **53,** 11818–11821 (2014).

Author contributions

C.-Y.S. and M.P. designed the research and wrote the paper. K.W. and K.L. carried out most of the syntheses and measurements. Y.-J.H., L.-Y.Z. and L.C. helped in experiments and data analyses. All authors discussed the results and commented on the manuscript.

Additional information